Infragravity wave frequency structure on a double-barred beach

Authors: Sénéchal, Nadia, Bonneton, Philippe, and Dupuis, Hélène

Source: Journal of Coastal Research, 36(sp1) : 654-661

Published By: Coastal Education and Research Foundation

URL: https://doi.org/10.2112/1551-5036-36.sp1.654

Journal of Coastal Research	SI 36	654-661	(ICS 2002 Proceedings)	Northern Ireland	ISSN 0749-0208

Infragravity wave frequency structure on a double-barred beach

Nadia Sénéchal†, Philippe Bonneton, and Hélène Dupuis

Department of Geology and Oceanography
UMR 5805
University of Bordeaux I
Avenue des Facultés
33405 Talence, cedex
France
†corresponding author: n.senechal@epoc.u-bordeaux.Fr

ABSTRACT

Low frequency waves, motions with typical frequencies of 0.001-0.05 Hz (also called infragravity or long waves) play an important role in many coastal sedimentary processes. So it is of considerable interest to improve our knowledge not only of their generation but also of their structure, in particular in very shallow water, where it has been shown that the wave energy spectrum can be dominated by long-period waves. Infragravity wave frequency structure on a transect crossing the surf zone of a fine grained, gently sloping double-barred beach was investigated using data from a 3-element coherent bottom-mounted pressure and current sensor line. In particular, it is shown that the infragravity wave frequency structure is largely controlled by the local bathymetry and appears to be unaffected (or at least not significantly) by water depth and wave breaking. In particular, the far infragravity band (< 0.01 Hz) is significant only at sensor situated landward of the ridge and runnel system and thus at all stages of the tide (water depth covering 0.6 m to 2.5 m) The nature of this far infragravity motion is not well understood. On the other hand, the 0.02-0.035 Hz band is linked to the difference nonlinear triad interaction associated with the two primary incident waves (peak frequencies centred around 0.06 Hz and 0.09 Hz).

ADDITIONALINDEXWORDS: *field experiment, sandy beach, surf zone, far infragravity, subharmonics*

INTRODUCTION

Since the observations by MUNK (1949), much effort has been devoted to investigate the source of low frequency waves, i.e. motions with periods at least twice that of the incident waves. Indeed, it is believed that these low frequency waves, with typical frequencies of 0.001-0.05 Hz (also called infragravity or long waves) play an important role in harbour oscillations, sediment transport and in determining the morphodynamics of beaches (HUNTLEY *et al.*, 1993; O'HARA and HUNTLEY, 1994). In general, infragravity wave energy is regarded as highly correlated with energy in the short-wave frequency band, indicating that the long-wave motions are locally driven by incident sea and swell (ELGAR *et al*., 1992; RUESSINK, 1998). The variance of infragravity band fluid motions can be divided into specific energy partitions associated with bound waves, leaky waves, edge wave modes and nongravity waves.

Bound waves have been found to contribute to infragravity wave energy (ELGAR and GUZA, 1985, RUESSINK, 1998). Ruessink (1998), showed that E_{bnd} / E_{ig} increased with higher H_{ss} / h (where H_{ss} is the significant sea swell wave height and h is water depth), reaching maximum values of up to 0.8 at the onset of short-wave breaking. Bound waves are generated through wave-wave nonlinear triad interactions. The nonlinear interaction between two free (i.e. obeying the dispersion relation) surface waves with frequencies f and f+Δf excite a forced secondary wave with the sum frequency 2f+Δf or the difference frequency Δf (with Δf in the infragravity frequency band). It was commonly hypothesized that the incident bound long waves were not destroyed in the surf zone but were released as free waves (LONGUET-HIGGINS and STEWARD, 1962). Recently, RUESSINK (1998) showed that wave breaking was associated with a rapid decrease in the ratio E_{bnd} / E_{ig} in the onshore direction and, consequently, with a rapid increase in the contribution of free infragravity energy to the total infragravity field.

After reflection at the shoreline the released waves propagate in a seaward direction and may either escape into deep water (leaky waves) or remain refractively trapped to the shore (edge waves).

Finally, oscillations in the longshore current are rapidly becoming recognised as an important form of infragravity motion. Recently, observations of a very low frequency

oscillation in the longshore current have been made by OLTMAN-SHAY *et al*. (1989), with typical frequencies of 0.001 Hz < f < 0.01 Hz (also called the far infragravity band). These longshore current oscillations have since become known as 'shear waves', and co-exist with bound, edge and leaky waves in the infragravity band.

The aim of our paper is to report observations of infragravity energy on a double-barred beach situated on the French Atlantic coastline in the presence of a low energy narrowband and long swell but also in the presence of high secondary wave generation due to nonlinear triad interactions. Emphasis will be placed on the evolution of the frequency structure of the infragravity band. Indeed, this structure appears to be largely controlled by the local bathymetry of the beach. Our paper is based on data collected during fieldwork in March 2000 (2 days) from a cross-shore line of 3 bottom-mounted pressure transducers on a gently sloping sandy barred beach known as Truc Vert.

STUDYAREA, MATERIALS AND METHODS

Study area

Truc Vert beach is situated on the southern part of the French Atlantic coastline. This is a low sandy coast, almost N-S orientated and bordered by high aeolian dunes. The sediment consists primarily of a medium grained quartz sand with a median particle size around 350 mm (LORIN and VIGUIER, 1987). Truc Vert beach is of the intermediate type 2e (following MASSELINK and SHORT, 1993) and generally exhibits a single ridge and runnel system in the dissipative lower intertidal domain and a steeper beach face. However, during the field experiment the beach exhibited two ridge and runnel systems in the dissipative lower intertidal domain (Figure 1).

This coast is exposed to almost continuous high energy swell originating mainly from the west-northwest. The high meso-macro tidal range, approximately 4.5 m at spring tides, along with the relatively broad intertidal region (around 200 m), allows instruments to be deployed and recovered safely at low tide while measurements can be obtained at high tide.

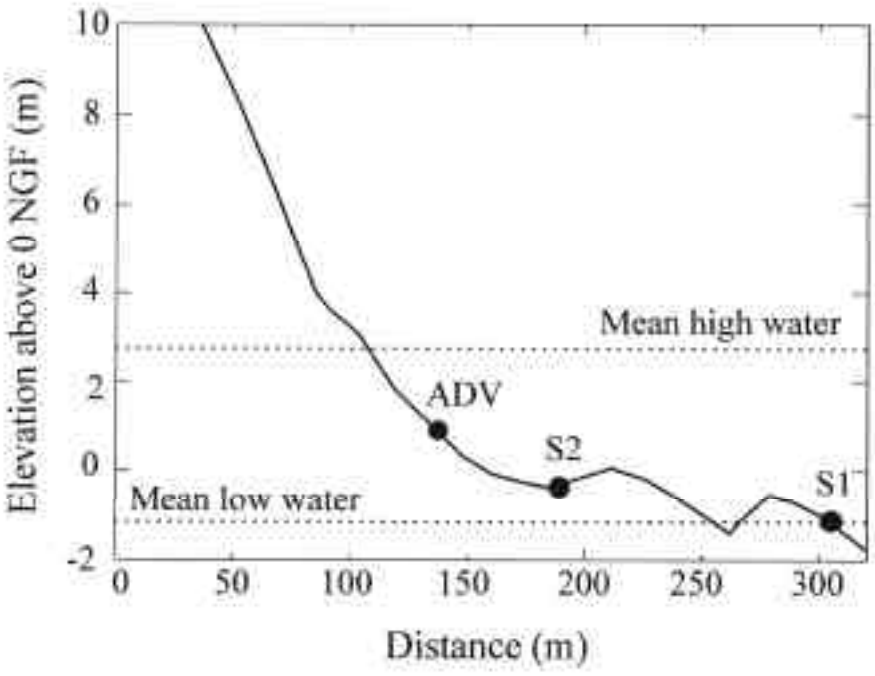

Figure 1. Beach profile and sensor deployment at Truc Vert beach on March 20th and 21st, 2001. S1 and S2 are the two bottom mounted Directional Wave Current Meters (InterOcean system) and ADV is the Acoustic Doppler Velocimeter vector (Nortek, AS).

Materials

Pressures were measured at three locations in the intertidal zone (Figure 1) using two bottom-mounted Directional Wave Current Meters (S1 and S2) from InterOcean system and one Acoustic Doppler Velocimeter (ADVvector) instrument from Nortek SA. The outer station (S1), situated in about 3.7 m water depth at high tide, served as the reference gage for the incident waves. The data were acquired at a 2 Hz sampling rate for the two Directional Wave Current meters (S1 and S2) and at an 8 Hz (the first day) and 32 Hz (the second day) sampling rate for the ADV (for further details, see SÉNÉCHAL *et al*. 2001b).

Methods

All hydrodynamic data were processed similarly. First, pressure measurements were converted to water elevations. Outside the surf zone, a correction factor as proposed in HORRIKAWA (1988) was applied to account for the pressure field being non-hydrostatic. This correction led to a high frequency cutoff of F_{hi} = 0.4 Hz. In the surf zone, sea surface elevations were estimated assuming that the pressure field is hydrostatic (LIN and LIU 1998). Power spectral and cross-spectral estimates were calculated using Fourier transforming overlapping (75%), Hanning-windowed, and detited 20-min data segments averaged over 60 minutes (d.o.f. = 18).

Over the 2 day field period, measurements were taken over two high tide cycles in the presence of low energy narrowband and long incident swell (peak period between 11 s and 14 s); waves were regular with a significant wave height (defined as 4 times the sea surface elevation standard deviation) of about 0.65 m the first day and 0.90 m the second day. The swell was propagating normally to the coast. On the first day, waves at high tide were breaking only on the beach face whereas on the second day, waves at high tide were generally breaking on the landward bar predominantly by plunging with a second breakpoint located on the beach face. For both days, two breakpoints (one on the landward bar and another on the beach face) were present during rising and falling tide.

RESULTS

Energy density spectrum evolution

Figure 2 provides an illustration of the energy density spectrum evolution at high tide between station S1 situated seaward of the double ridge and runnel system (black line) and station S2 situated landward of the double ridge and runnel system (grey line). We clearly observe that a bulge of high-frequency energy becomes increasingly important between station S1 and station S2. The energy at these frequencies is relatively broad banded but appears to be centered on frequencies corresponding to harmonic frequencies. This is consistent with previous work (ELGAR *et al*., 1997; NORHEIM *et al*., 1997 and many others). SENECHAL *et al*. (2001b, 2001c) showed that this energy has been first transferred from the primary to the harmonic frequencies through nonlinear wave-wave interactions and then has been released, leading to secondary wave generation landward of the double ridge and runnel system. Associated with this phenomenon of harmonic release, they observed a decay by a factor 1.5 of the significant wave period.

Concerning the low frequency band (T > 20 s), we observe the modification of the energy density spectrum structure. The total energy in this band only slightly increases by a factor less than 1.5 between station S1 and station S2 but it is redistributed into two components at station S2: the first one corresponding to periods greater than 100 s (frequencies < 0.01 Hz) and the second one corresponding to periods between 30 s and 50 s (0.02 Hz < frequencies < 0.035 Hz). The low frequency band has been divided into four components: the so called far infragravity band (f < 0.01 Hz), the 0.01-0.02 Hz component, the 0.02-0.035 Hz component and the 0.035-0.05 Hz component. Focusing on the evolution of the most energetic component both in time and in space, it will be shown below that the

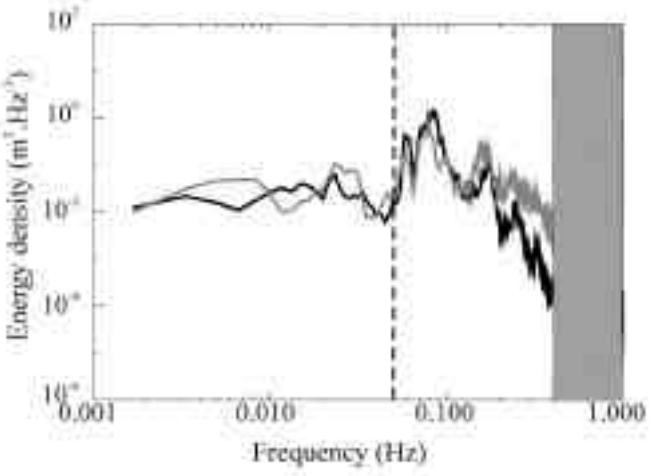

Figure2. Typical power spectra calculated by Fourier transforming overlapping (75%), Hanning-windowed, and detited 20-min data segments averaged over 60 minutes (d.o.f. = 18) at high tide at station S1 (black line) and station S2 (grey line). The vertical dashed line indicates the boundary between high frequency and infragravity waves. We can observe the increase in height frequency energy and the bimodal structure of the infragravity band at station S2.

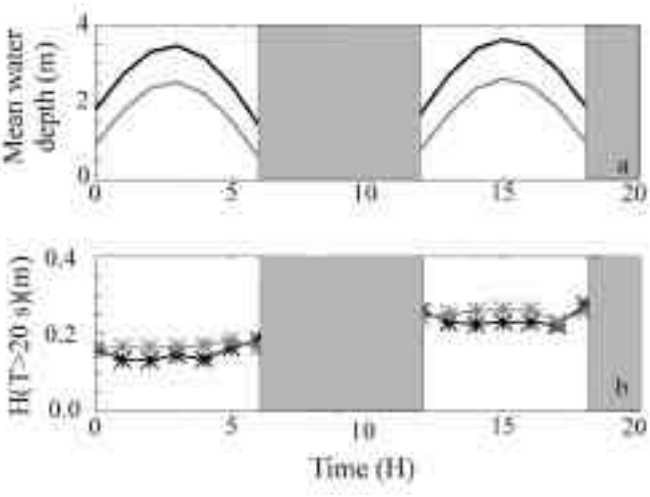

Figure 3. (a) Mean water depth, computed over one hour, versus time (in black: S1 and in grey: S2). (b) Low frequency (f < 0.05 Hz) significant wave heights (computed from the integration of the energy density spectrum in the low frequency band) versus time. The grey rectangle corresponds to the time when the stations were not fully immersed.

low frequency structure at station S2 is observed over all stages of both tides for water depths ranging 0.6 m to 2.5 m in both breaking and nonbreaking conditions.

Figure 3a shows the mean water depth evolution during the two tides and Figure 3b shows the evolution of the low frequency significant wave heights (computed from the integration of the energy density spectrum in the low frequency band). First, we observe a slight increase of the low frequency significant wave heights between the two tides. This is due to the increase of the significant wave height (0.65 m the first day versus 0.90 m the second day). This observation is consistent with previous work (RUESSINK, 1998). Second, we observe that the low frequency significant wave heights at station S2 (grey star) and station S1 (black star) remain relatively constant during all stages of the tide. This implies that the slight energy increase observed in the low frequency band between the two stations (see Figure 2) is not due only to the decrease in water depth but this also implies that the total energy at low frequencies is not affected by breaking. Indeed on the first day, waves at high tide were breaking only on the beach face whereas on the second day, waves were generally breaking on the landward bar and then on the beach face. So, on the first day station S2 was not always situated in the surf zone. This is similar to the result established by SÉNÉCHAL *et al.* (2001c) on the same data set but concerning the high frequency energy. They showed that wave breaking did not affect (or at least not significantly) energy transfer to higher frequencies. Figure 3 also implies that the low frequency significant wave heights at station S1 and station S2 remained relatively constant in the surf zone. Indeed, during rising and falling tide, two breakpoints were present and so station S2 was always well in the surf zone. This is consistent with a previous result established in the same study area with weak irregular waves present (significant wave heights were less than 1.2 m and wave periods were around 8 s) and sensors deployed outside the influence of the ridge and runnel system (SÉNÉCHAL *et al*., 2001a). This is also consistent with the work of RUESSINK (1998) whose his entire measurements transect, deployed on a double barred beach, experienced surf zone conditions (wave heights about 2-3 m).

Low frequency energy structure

Figure 4a shows the mean water depth evolution, while Figure 4b and Figure 4c respectively show the evolution of the two most energetic low frequency components relative to the total low frequency energy at stations S1 and S2: the 0.01-0.02 Hz component (triangle), the 0.02-0.035 Hz component (star) and the far infragravity component (diamond). It can be seen from Figure 4b that at station S1 at least 70 % of the low frequency band energy is contained in the 0.01-0.02 Hz and in the 0.02- 0.035 Hz frequency bands; this proportion remains roughly constant during all

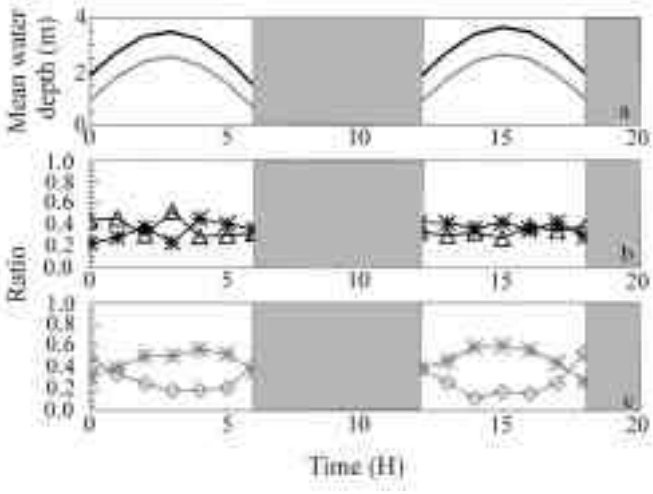

Figure 4. (a) Mean water depth, computed over one hour, versus time (in black: S1 and in grey: S2). (b) Ratio of selected frequency band energy to total infragravity energy versus time at station S1: 0.01-0.02 Hz frequency band (triangle) 0.02-0.035 Hz frequency band (asterisk). (c) Ratio of selected frequency band energy to total infragravity energy versus time at station S2: 0.001-0.01 Hz frequency band (diamond) 0.02-0.035 Hz frequency band (asterisk).

stages of the tide. In contrast Figure 4c shows the mean water depth dependence of the low frequency energy structure at station S2: the far infragravity (0.001-0.01 Hz) relative energy component increases when the mean water depth decreases and conversely the 0.02-0.035 Hz relative energy increases when the mean water depth increases. At station S2, at least 80 % of the low frequency band energy is contained in the far infragravity band and in the 0.02-0.035 Hz component but their proportions are not the same during the tide. So, even though the total low frequency energy appears to be independent of the local water depth at stations S1 and station S2 (Figure 3), the low frequency energy structure at station S2 is dependent on the local water depth (Figure 4c). In contrast at the seaward station S1 the low frequency energy structure is clearly independent of the local mean water depth as illustrated by Figure 4b.

The energy associated with the far infragravity band can be observed at station S2 in the time domain records as illustrated in Figure 5. This figure shows the sea surface elevation as measured at station S1 (Figure 5a) and at station S2 (Figure 5b) when the two stations are almost in the same mean water depth. The black line is the smoothed time domain record, with a smoothing window of 65 seconds (about 5 primary wave periods). We observe in Figure 5b a strong low frequency modulation of the mean sea surface elevation, which seems to be developed when the mean water depth decreases whereas at station S1 (Figure 5a), this long motion is much lower (in contrast the modulation associated with the wave groups are more marked).

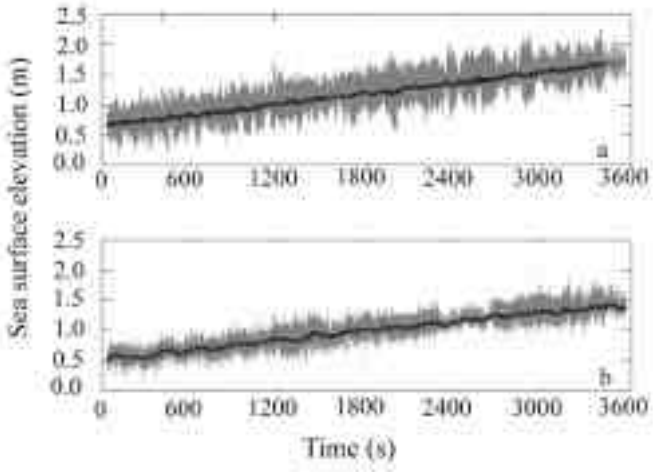

Figure 5. Sea surface elevation time series as measured at (a) station S1 and (b) station S2. The black solid line represents the smoothed time series using a smoothing window of 65 s (about 5 primary wave periods).

Figures 4 and 5 show that the far infragravity energy is locally generated or at least amplified, probably due to the influence of bathymetry, and also that this far infragravity energy is associated with a decrease in water depth. In contrast the 0.02-0.035 Hz subharmonic component does not appear to be directly linked to the bathymetry.

Coherence and phase

Figures 6 and 7 show the evolution of the coherence (b) and the phase (c) between the sea surface elevation time series and the cross-shore velocities in the far infragravity frequency band (Figure 6) and in the 0.02-0.035 Hz frequency band (Figure 7) at station S1 (black asterisk) and at station S2 (grey asterisk). Each asterisk represents the mean coherence/phase in the selected frequency band and the vertical bars represent the standard deviation associated with this mean value. In other words, this vertical bar represents the variability of the coherence/phase across the frequency band.

For the far infragravity band the coherence between the cross-shore velocity and the sea surface elevation time series increases between station S1 and station S2 from 0.3-0.4 to 0.7-0.8 (Figure 6b) and the standard deviation is relatively small, suggesting that the two time series are highly correlated across the far infragravity band at station

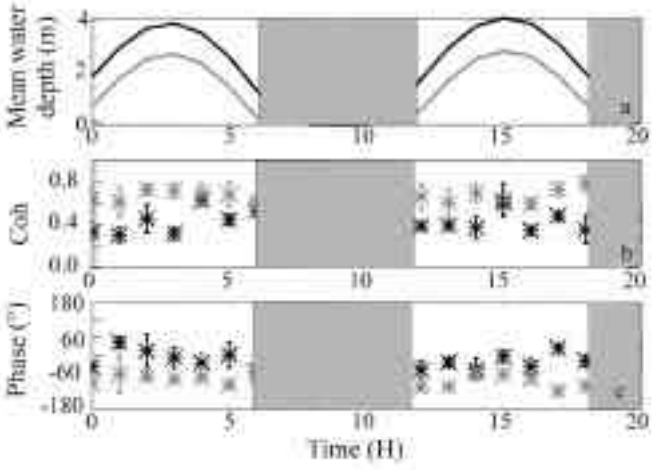

Figure 6. (a) Mean water depth, computed over one hour, versus time (in black: S1 and in grey: S2). (b) Mean coherence computed over the far infragravity band (f < 0.01 Hz) at station S1 (black asterisk) and station S2 (grey asterisk) versus time. The vertical error bar denotes the standard deviation. (c) Mean phase computed over the far infragravity band (f < 0.01 Hz) at station S1 (black asterisk) and station S2 (grey asterisk) versus time. The vertical error bar denotes the standard deviation.

S2. Furthermore, at station S2, the coherence is less variable in time than is the coherence at station S1. This underlines the local behavior of the far infragravity band, which appears to be related to the influence of bathymetry. The phase between the cross-shore velocity and the sea surface time series is nearly –90 ° at sensor S2 (Figure 6c), during all the experiments and again the standard deviation associated with this value is relatively low. This value of –90 ° is typical of the standing wave motions.

Figure 7b deals with the 0.02-0.035 Hz frequency band. We can see that the coherence between the cross-shore velocity and the sea surface elevation time series increases between station S1 and station S2 from 0.5-0.6 to 0.7-0.8 and that the standard deviation is relatively weak, suggesting that the sea surface elevation and the cross-shore velocity time series are highly correlated across the 0.02-0.035 Hz band at both stations S1 and S2. The phase between the cross-shore velocity and the sea surface time series is close to 0° at both stations during all the experiments and again the standard deviation associated with this value is relatively low (Figure 7c). This value of 0 ° suggests that the energy contained in this frequency band is a wave propagating motion.

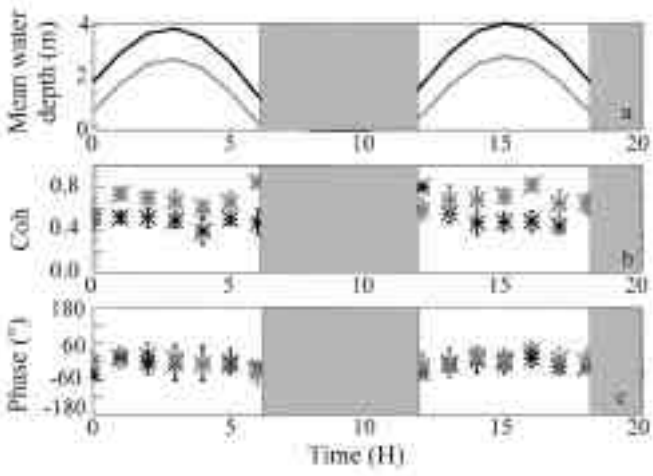

Figure 7. (a) Mean water depth, computed over one hour, versus time (in black: S1 and in grey: S2). (b) Mean coherence computed over the 0.02-0.035 Hz frequency band at station S1 (black asterisk) and station S2 (grey asterisk) versus time. The vertical error bar denotes the standard deviation. (c) Mean phase computed over the 0.02-0.035 Hz frequency band at station S1 (black asterisk) and station S2 (grey asterisk) versus time. The vertical error bar denotes the standard deviation.

DISCUSSION

The 0.02-0.035 Hz band

The 0.02-0.035 Hz band is significant at station S1 but also at station S2 and represents one of the greatest contributions to the total low frequency band energy (Figure 4). The coherence between the sea surface elevation and the cross-shore velocity time series is high at all stages of the tide. Furthermore the two time series are in phase in this frequency band. The 0.02-0.035 Hz band is here certainly associated with the difference interactions between the two primary frequencies observed in the spectra (Figure 2): the first one centred around 0.06 Hz and the second one centred around 0.09 Hz.

Indeed, SÉNÉCHAL *et al*. (2001b, 2001c), using higher order spectral analysis (the bispectrum) have shown that nonlinear sum triad interactions were very important in this data set, leading to significant energy transfer to the higher frequency components. This high frequency energy, at first bound to the primary waves, was then partially released landward of the ridge and runnel system in both breaking and non breaking conditions. Nevertheless, all the energy is not necessarily transferred to higher frequency components and a proportion can also be transferred to lower frequencies through difference interactions. RUESSINK (1998), using a bispectral technique on recordings of near-bottom pressure obtained at three positions on a gently sloping multiple-bar system showed that forced waves are the main source of free infragravity motions. He also noted that free infragravity energy might also be generated in the absence of breaking waves.

Nevertheless, at this stage it is not possible to determine if these waves are free onshore propagating waves, leaky or edge modes (indeed, at these frequencies, wave reflection at the shoreline can become relatively important). A field experiment conducted on the same beach on October 2001 should allow us, using wavenumber-frequency spectra as proposed in HOLLAND and HOLMAN (1999), to clearly identify the various wave types.

The far infragravity band

Low frequency energy in the surf zone has been measured at many experiment sites, and oscillations in the longshore current have been recognised as an important form of infragravity motion. These longshore current oscillations have since become known as "shear waves", and co-exist with edge, leaky and standing waves in the infragravity band. Furthermore, OLTMAN-SHAY *et al*. (1989) suggested that shear waves dominate oscillations in velocity in the region of the far infragravity band.

During all the experiments longshore current velocities were relatively low: at station S1, the mean longshore current was around 0.1 m/s during the entire field

experiment and at station S2, situated in the runnel, it was around 0.25 m/s. Figure 8 represents (a) the mean water depth evolution (b) the total velocity variance (0.001-0.4 Hz) and (c) the far infragravity velocity variance (0.001-0.01 Hz) at station S1 (black symbol) and station S2 (grey symbol). First, like for the low frequency wave height (Figure 3), we observe a slight increase of total longshore velocity variance between the two tides, which can be linked to the increase in the significant wave height. Second, Figure 8b clearly illustrates the depth dependence of the total longshore velocity variance at station S2 and on the other hand its low depth dependence at station S1. Figure 8c shows the strong depth dependence of the far infragravity band to the total longshore velocity variance at station S2 whereas at station S1 this depth dependence is noticeable only when the sensor is in very shallow water. The evolution of the far infragravity contribution to the total longshore velocity variance is similar to the evolution of the far infragravity band in the sea surface time series. One can think that the far infragravity component at station S2 is associated with shear waves and that the presence of the runnel stresses these waves. Nevertheless the strong coherence between elevation and cross-shore velocity at station S2 (Figure 6b) and the phase of –90° also suggest the presence of a standing wave motion during all tidal stages. The reasons for this are not well understood.

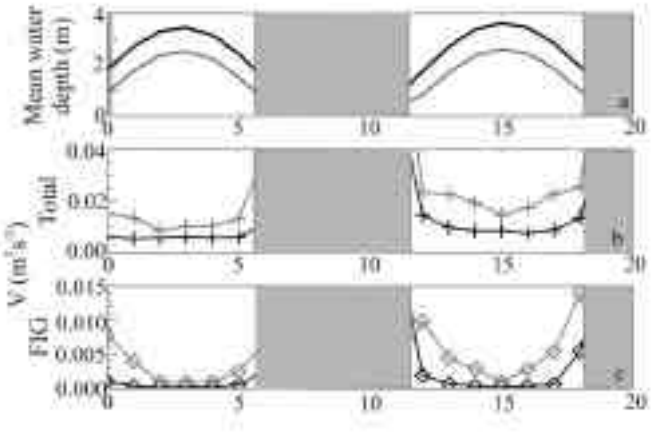

Figure 8. (a) Mean water depth, computed over one hour, versus time. (b) Total longshore velocity variance versus time at station S1 (black cross) and station S2 (grey cross). (c) Far infragravity longshore velocity variance versus time at station S1 (black diamond) and station S2 (grey diamond).

CONCLUSIONS

A field experiment conducted on a double-barred beach on the southern part of the French Atlantic coastline allowed us to investigate the frequency structure of the infragravity wave variance. Conditions were typical of low energy (significant wave height less than 1.0 m in about 3.7 m water depth), narrowband and long swell (peak period around 11-14 s). Nonlinear triad interactions were strong, leading to significant energy transfer to higher harmonics.

Figure 3 shows that the low frequency significant wave heights at stations S1 and S2 remain relatively constant during all tidal stages, implying in particular that the total energy at low frequencies is not affected by breaking. On the other hand, it is clear from Figure 4 that the frequency structure of the infragravity band is different at stations S1 and S2: the two most energetic frequency bands at station S1 are the 0.01-0.02 Hz component and the 0.02-0.035 Hz component whereas at station S1, the two most energetic bands are the far infragravity component (< 0.01 Hz) and the 0.02-0.035 Hz component. Furthermore, Figure 4 shows that the frequency repartition at station S2 is dependent on the mean water depth whereas at station S1 it is not.

Analysis of cross spectra between elevation and cross-shore velocity show high coherence levels in the far infragravity band and in the 0.02-0.035 Hz band (Figures 6b and 7b). The phase in component 0.02-0.035 Hz is close to 0° at stations S1 and S2 whereas the phase in the far infragravity band at station S2 is close to $-90°$.

Thus, since the 0.02-0.035 Hz band is significant at station S1 but also at station S2 and represents one of the greatest contributions to the total low frequency band energy (Figure 4), it has been linked to the difference nonlinear triad interaction between the two primary incident wave peaks (Figure 2). Nevertheless at this stage it is not possible to determine if these waves are free onshore propagating waves, leaky or edge modes (indeed, at these frequencies, wave reflection at the shoreline can become relatively important).

Concerning the far infragravity band, which is significant only at station S2, shear waves could probably explain their increased significance in very shallow water depths (see Figure 8b); the presence of the runnel (S2 is situated in the runnel) probably amplifies these waves. Nevertheless the strong coherence between elevation and cross-shore velocity at station S2 (Figure 6b) and the phase of –90° also suggest the presence of a standing wave motion during all tidal stages. The reasons for this are not well understood.

Acknowledgments

This study was performed within the framework of the Programme National d'Environnements Côtiers, project "Hydrodynamique sédimentaire en zone côtière", sponsored

by CNRS/INSU. Partial support was also received from the European community under MASTcontract N°. MAS3-CT-0106. We would like to thank Mr. A. de Resseguier, Mr. G. Oggian and Mr. R. Butel for their contributions.

LITERATURE CITED

ELGAR, S. and GUZA, R.T., 1985. Observations of bispectra of shoaling surface gravity waves. *Journal of Fluid Mechanics*, 161, 425-448.

ELGAR, S.; HERBERS, T.H.C.; OKIHIRO, M.; OLTMAN-SHAY, J., and GUZA, R.T., 1992. Observations of infragravity waves. *Journal of Geophysical Research*, 97, 15,573-15,577.

ELGAR, S.; GUZA, R.T.; RAUBENHEIMER, B.; HERBERS, T.H.C., and GALLAGHER, E.L., 1997. Spectral evolution of shoaling and breaking waves on a barred beach. *Journal of Geophysical Research*, 102 (C7), 15,797-15,805.

HOLLAND, K.T. and HOLMAN, R.A., 1999. Wavenumber-frequency structure of infragravity swash motions. *Journal of Geophysical Research*, 104 (C6), 13,479-13,488.

HORRIKAWA, K., 1988. *Nearshore Dynamics and Coastal Processes*. Part V Chapter 2, 386-406.

HUNTLEY, D.A.; DAVIDSON, M.; RUSSELL, P., FOOTE, Y., and HARDISTY, J., 1993. Long waves and sediment movement on beaches: recent observations and implications for modelling. *Journal of Coastal Research*, 15, 215-229.

LIN, P. and LIU, P.L.-F., 1998. A numerical study of breaking wave in the surf zone. *Journal of Fluid Mechanics*, 359, 239-264.

LONGUET-HIGGINS, M.S. and STEWARD, R.W., 1962. Radiation stress and mass transport in surface gravity waves with application to "surf beats". *Journal of Fluid Mechanics*, 13, 481-504.

LORIN, J. and VIGUIER, J., 1987. Hydrosedimentary conditions and present evolution of Aquitaine Coast. *Bull. Inst. Geol. Bassin Aquitaine* 41.

MASSELINK, G. and SHORT, A.D., 1993. The effect of tide range on beach morphodynamics: a conceptual model. *Journal of Coastal Research*, 9, 785-800.

MUNK, W.H., 1949. Surf beat. *EOS, Trans. AGU*, 30, 849-854.

NORHEIM, C.A.; HERBERS, T.H., and ELGAR, S., 1997. Nonlinear evolution of surface wave spectra on a beach. *Journal of Physical Oceanography*, 28, 1534-1551.

O'HARA, T.J. and HUNTLEY, D.A., 1994. Bar formation due to wave groups and associated long waves. *Marine Geology*, 116, 313-325.

OLTMAN-SHAY, J.; HOWD, P.A., and BIRKEMEIER, W.A., 1989. Shear instabilities of the mean longshore current. 2. Field observations. *Journal of Geophysical Research*, 94, 18,031-18,042.

RUESSINK, B.G., 1998. Bound and free infragravity waves in the nearshore zone under breaking and nonbreaking conditions. *Journal of Geophysical Research*, 103 (C6), 12,795-12,805.

SENECHAL, N.; DUPUIS, H.; BONNETON, P.; HOWA, H., and PEDREROS, R., 2001a. Observation of irregular wave transformation in the surf zone over a gently sloping sandy beach on the French Atlantic coastline. *Oceanologica Acta*, 24 (6), 545-556.

SENECHAL, N; BONNETON, P., and DUPUIS, H., 2001b. Field experiment on secondary wave generation on a barred beach and the consequent evolution of energy dissipation on the beach face. *Coastal Engineering* (in review).

SENECHAL, N.; BONNETON, P., and DUPUIS, H., 2001c. Generation of secondary waves due to wave propagation over a bar: a field investigation. *Proceedings of WAVES'01* (San Francisco, USA, ASCE).